RSC Advances

ROYAL SOCIETY OF CHEMISTRY

www.rsc.org/advances

,

Novel pervoskite-spinel composites approach to enhance magnetization of $LaFeO_3$

Vishwajit M. Gaikwad, and Smita A. Acharya

Department of Physics, Rashtrasant Tukadoji Maharaj Nagpur University, Nagpur 440033, India.

In the present attempt, perovkite-spinel interface effect on bulk magnetic behavior of lanthanum ferrites ($LaFeO_3$) based composites system is under investigation in view of enhancement of magnetization of $LaFeO_3$. The composite system by using $LaFeO_3$ as perovskite phase and $NiFe_2O_4$ as spinel phase with compositions (x = 0, 20, 30, 40 and 100 wt%) are developed by mechanical mixing. Structures are confirmed by using X-ray diffraction (XRD) and Fourier Transform Infrared Spectroscopy (FTIR). Physical interaction of $LaFeO_3$ and $NiFe_2O_4$ phases at interface are realized by XRD peak broadening and shifting. M-T and M-H curves are closely monitored to investigate the perovskite-spinel interface effect on bulk magnetic behavior of the composites. Significant enhancement in magnetization in perovskite-spinel composite phase for 60%$LaFeO_3$-40%$NiFe_2O_4$ composition over individual phases are detected. The composition effect up to 60:40 of $LaFeO_3$-$NiFe_2O_4$ is considered to preserve dominancy of $LaFeO_3$ phase. The spin coupling mechanism across interface is speculated for the enhancements of magnetization in composite. Mossbauer spectroscopy investigation confirms co-existence of magnetization in composites.

Introduction

Current trend in materials research is intensively focused on the development of complex oxide composite to create new functional performance and improve the existing ones. Interfaces of composite plays a key role in modulating effective material properties and thus improve functionality[1]. Role of interface is primarily important because enhancement in the properties of composites results from the interaction of component phases at the interface[2]. Several phenomena occur at the interfaces i.e. rearrangement of chemical bonding[3]; spin, charge and orbital reconstruction;[4] modification in electronic structure[5] etc.

Combination of perovskite-spinel system seems to be very promising for multifunctional or multiferroic properties[6]. Elastic coupling between them plays major role to observe magnetoelectric coupling[7]. Perovskite-spinel interface is also of great interest in complex oxide based magnetic tunnel junctions[2]. Several combinations have been extensively

,

studied by taking $BiFeO_3$ and $BaTiO_3$ as perovskite and exploited their magnetic and magnetoelectric response[8-15]. Using $LaFeO_3$ (LFO) as perovskite, significant magnetization was observed in its superlattices[16,17]. But, the combination of perovskite LFO with spinel system is very rare. In this letter, we have taken an attempt to study enhancement in magnetization when perovskite LFO combines with spinel phase. LFO is the member of rare earth orthoferrite family. It has orthorhombic perovskite structure (space group:Pbnm) and exhibited phase transition from orthorhombic to rhombohedral at T~1260 K[18]. LFO possesses G-type antiferromagnetism (T_N ~738 K) in which inter and intralayer spin couplings are antiparallel. It also shows Fe^{3+}-O-Fe^{3+} superexchange interaction. Fe^{3+} is in its high spin state (t_{2g}^3, e_g^2).[19,20] LFO has various promising applications in solid oxide fuel cell, catalysts, chemical sensors etc[21]. LFO can be exploited as room temperature multiferroic as an alternative of $BiFeO_3$ but its functionality is limited by low magnetization.

Bulk $NiFe_2O_4$ (NFO) is well known soft ferrimagnetic insulator with inverse spinel structure. It ferrimagnetic ordering temperature is around T_c ~ 850 K.[22-24] Within inverse spinel structure, Fe^{3+} ions are occupied at tetrahedral site in sublattice A. Ni^{2+} and Fe^{3+} ions are located at octahedral site in sublattice B. It means, Fe^{3+} ions are equally distributed in tetrahedral as well as octahedral site inside inverse spinel structure. Magnetic structure of NFO consists of antiferromagnetic coupling between two sublattices A and B. With this ordering, moment of Fe^{3+} ion at A and B site cancel out and leaves behind $2\mu_B$/f.u. magnetic moment which arises only due to Ni^{2+}.[22-24,25] Magnetic interaction (Fe-Fe superexchange interaction) plays an important role to determine its utility in disk recording or fabrication of magnetic cores of read/write head for high speed digital tape.[26,27] This background motivates us to develop LFO-NFO composites system to investigate interface effect on magnetic behavior. Main purpose of the study is enhancement of magnetization of LFO system, so composite effect up to 60%LFO-40%NFO compositions are studied so that the dominancy of LFO phase could be preserved.

Experimental

Polycrystalline LFO and NFO compounds were synthesized separately by gel combustion and hydrothermal route, respectively. Both the systems were mechanically grounded to form $(1-x)LaFeO_3$-$xNiFe_2O_4$ (x = 20, 30, & 40%) powder composites. Lanthanum nitrate [$La(NO_3)_3.6H_2O$,99.9% pure, Sigma-Aldrich], Iron nitrate [$Fe(NO_3)_3.9H_2O$,99.9% pure, Sigma-Aldrich], Nickel nitrate [$Ni(NO_3)_2.6H_2O$, 99% pure,

,

Sigma-Aldrich], Sodium hydroxide flakes [NaOH, 90% Merck], and Glycine were used as precursors. LFO was synthesized by microwave-assisted sol gel combustion route. Ragatech microwave synthesis assembly was used to synthesize LFO. It consists of microwave processor of size 360 mm x 210 mm x 430 mm dimensions with a 2.45 GHz frequency multimode source having maximum deliverable power out-put as 700 W. Lanthanum nitrate and iron nitrate in stoichiometric (1:1) proportions were dissolved in double distilled water and stirred for 15 minutes. Then, 4 mole of Glycine was added into the prepared solution. The resultant solution was evaporated in microwave synthesis assembly at 210 W power until gelification. The resultant gel was combusted at same power level. After combustion, yellowish powder was formed within few seconds. The as-synthesized powder was calcined at 600^0C for 3 hours (optimized condition) to get final product as polycrystalline LFO.

NFO was synthesized by hydrothermal synthesis route. Stoichiometric amount of nickel nitrate and iron nitrate were dissolved in 100 ml double distilled water. This solution was stirred for 30 minutes. Then, pH of solution was adjusted to 13 by dropwise addition of 2M NaOH solution into it. After adjusting pH, the solution was transferred into sealed Teflon stainless steel autoclave and then placed in hot air oven at 160^oC for 18 h. After the hydrothermal reaction, autoclave was allowed to cool naturally. The resultant precipitate (insoluble in water) was separated by centrifugation and washed with distilled water in sequence to remove water soluble salts. Then, precipitate was dried at 80^oC in oven to get final powder as polycrystalline NFO. Both these compounds were mechanically grounded in appropriate proportion to form (1-x)LFO-xNFO (x = 10, 20, 30, & 40 wt%) of powder composites.

X-ray powder diffraction measurements of composites were performed using a PANalytical Empyrean X-ray diffractometer equipped with a copper target (CuKα ~1.5406A˚). Diffraction data was collected in the range 20^o-80^o with step size 0.01973^o for step time 46.5 ms. The obtained diffraction data was refined using Rietveld refinement method with the help of Full Prof suite. Fourier Transform Infrared Spectroscopy was carried out by Bruker spectrometer (Germany, Model: Vertex70) having resolution ~0.5 cm^{-1} and λ~ 0.01 cm^{-1}. FTIR measurements were done within far IR range from 50 to 680 cm^{-1} at room temperature. The field and temperature dependent magnetization measurement were performed using Quantum Design MPMS Superconducting Quantum Interference Device (SQUID), Vibrating Sample Magnetometer. [Specification: Magnetic field upto 70kOe; Temperature range:350-1000K; Field charging rate : 4 to 700 Oe/sec.]. ^{57}Fe Mossbauer

,

spectra of LFO, NFO and their composites were recorded using Mossbauer spectrometer operated in constant acceleration mode in transmission geometry at RT. Source was employed ^{57}Co which further decay into ^{57}Fe. The calibration of velocity scale was done by using enriched ^{57}Fe metal foil.

Results and discussion

A. Structural confirmation

X-ray diffraction patterns for pure LFO, NFO and LFO-NFO composites are shown in Fig.1. XRD pattern of pure LFO is indexed as orthorhombic phase (JCPDS file no. 74-2203) while of NFO is matched with cubic spinel phase (JCPDS file no.89-4927) without any traces of impurities. LFO and NFO retains their respective structure and phase in LFO-NFO composite form. This is as expected because both the phases synthesized separately. However, broadening and shifting of LFO peaks [see Fig. 1(b)] with increasing NFO concentration are evidence for physical interaction of interface of LFO-NFO. In addition to that, the peak corresponds to spinel phase along (311) direction appears stronger with increasing concentration of NFO in composites [see Fig. 1(c)] are clear indication of formation of perovskite-spinel mixed structure[5,8]. Rietveld refinement of X-ray diffraction patterns reveal orthorhombic (space group:Pbnm) symmetry for LFO and inverse spinel cubic (space group: Fd3m) symmetry for NFO [See Fig 2]. Refined lattice parameters a = 5.5581(7) A^o, b = 5.5722 (8) A^o and c = 7.8601(11) A^o for LFO and a = b = c = 8.349 (6)A^o for NFO are comparable with literature.[28]

The local structure of the composite systems is probed by FTIR technique. FTIR spectra for pure LFO, NFO and LFO-NFO composites taken between 50 - 680 cm^{-1} are shown in Fig. 3. According to symmetric calculations, orthorhombic Pbnm phase (for LFO) should possess 25 IR active optical phonon modes [$9B_{1u}+7B_{2u}+9B_{3u}$) in the range 115 - 645cm^{-1}.[28,30] In present study, from the FTIR spectra of LFO (Fig 3a), 8 broad vibrational modes are identified. Modes below 200 cm^{-1} (ν_1 & ν_2) can be assigned to La^{3+} vibrations. Strong absorption peak at 170 cm^{-1}(ν_2) can be assigned to 'external' phonon mode, which arises due to vibration of La^{3+} ions against FeO_6 octahedra[31]. Absorption bands between 200-300 cm^{-1} (ν_3 & ν_4) can be referred as oxygen octahedral tilting modes.[32] Broad absorption peak (ν_5) near 350 cm^{-1} is correlated with Fe^{3+}-O^{2-} bending vibrations.[33] Transverse optic (TO) mode B_{1u} (ν_6) observed at 441 cm^{-1} is associated to O-Fe-O deformation vibration of perovskite LFO and band (TO, B_{3u}) at 540 cm^{-1} (ν_7) is related to iron-oxygen (Fe-O)

,

stretching vibrations.[30,32,33] Small shoulder (ν_8) appears at 600 cm^{-1} is the characteristic feature of rare earth orthoferrites.[33]

Fig 3b exhibits FTIR spectra of NFO. In spinel structure, lower energy bands can be assigned to intrinsic stretching vibrations of metal-oxygen bond at tetrahedral site whereas higher energy bands can be correlated to metal-oxygen bond at octahedral site.[34] For NFO, characteristic absorption peak at 603 cm^{-1} (ν_6') can be associated to stretching vibrations of $(Fe\text{-}O)_{tetra}$ bond which is the main feature of spinel ferrite. Band in the form of shoulder at 550 cm^{-1} (ν_5') is also a sign of stretching vibrations of tetrahedraly coordinated Fe^{3+}-O^{2-} bond. Broad band observed near 400 cm^{-1}(ν_4') is related to stretching vibrations of Ni-O bond at octahedral site.[34-39] Weak absorption bands observed at 110, 191 and 270 cm^{-1} arises due to vibration of Fe^{3+} cations at octahedral site.[34,40] Higher energy modes of spinel structure (NFO) and lower energy modes of perovskite (LFO) both appear in FTIR spectra of composites (Fig.3c & d). No new vibrational modes are detected due to interface effect. It means there is no structural modulation across the interface after mixing individual phases of LFO and NFO. LFO and NFO are retained their identity in prepared composites.

B. Magnetic field and temperature dependent magnetization

Magnetic field dependence magnetization (M-H curve) of LFO, NFO and LFO-NFO composites at room temperature (R.T.~300K) are shown in Figs 4(a & b). Magnified view of M-H curve for LFO [Fig 4(b)] shows weak ferromagnetic nature with very less remnance magnetization (M_r ~ 0.0005 emu/g). Actually bulk LFO possess G-type AFM with canted Fe^{3+} spin.[41,42] The weak ferromagnetism is due to partial alignment of canted Fe^{3+} spin. Same magnetic behaviour of LFO was earlier observed by.[43] Magnetic hysteresis of NFO shows large saturation magnetization (M_s ~ 48.80 emu/g). Nature of magnetic ordering may be either ferrimagnetic or ferromagnetic. It is very difficult to distinguish between ferro and ferrimagnetic with SQUID-VSM measurements. This difficulty has been sorted out by measuring Mossbauer spectra of NFO. This will be discussed later on. For composite systems, remanent (M_r) as well as saturation (M_s) magnetization are found to be rised as compared to LFO-phase and continuously increasing with weight percentage of NFO. The M_r, M_s and squareness ratio (R) values of all systems are tabulated in Table 1. Squareness ratio (R) for LFO and composites is calculated by dividing M_r with M_s. Significance of R is to determine the type of intergrain exchanges[42]. Non zero values of R for LFO-NFO composites [see Fig.4(c)] experimentally prove intergrains magnetostatical interaction across

,

LFO and NFO interface. On the other hand, coercivity (H_c) of the composites system is found lower than pure LFO indicating soft magnetic behavior of composites as compared to LFO.

Role of interface magnetization on M_r and M_s values of composites can also be confirmed by estimating their values by using conventional Vegard's law approximation[5] as $M_{cal} = M_{LFO}(1 - x) + M_{NFO}(x)$, where M_{cal}, is estimated remanent magnetization of composite, while M_{LFO} and M_{NFO} are observed remanent magnetization of LFO and NFO single phase, respectively. The observed and calculated comparative plot of remanent magnetization with the wt% composition of NFO is shown in inset of Fig. 4(a). Surprisingly, observed remanent magnetization values for initial two compositions (20%NFO and 30%NFO) are found to be lower than calculated ones. However for the composition (40%NFO) remanent magnetization ($M_r \sim 4.49$ emu/g) is found higher than the calculated one ($M_r \sim 3.06$ emu/g). Almost same trend is observed for saturation magnetization also. The magnetic coupled interactions at interface of LFO-NFO composite are exclusively responsible for the enhancement in this composition. This confirms the modulation of spin-alignment at the interface of LFO-NFO composites as compared to their individual phases.

To get more clarity of the understanding of modulation of spin-coupling at the interface; the mechanism of spins alignments across the interface are speculated as shown in Fig 5. Individually, LFO has weak magnetization due to canting of Fe^{3+} spin magnetic moments. NFO has inverse spinel structure with ferrimagnetic ordering. Spin magnetic moments of Fe^{3+} positioned at octahedral lattice sites is anti-parallel with Fe^{3+} at tetrahedral lattice sites. Therefore, net contribution of magnetization due to Fe^{3+} spins is canceled out (as shown in Fig 5). Saturation magnetization of ferrimagetic NFO is only due to Ni^{2+} spins[22-25] which is aligned parallel at octahedral lattice sites. At bulk interface of LFO-NFO composites, spin reconstruction of LFO and NFO domains take place. Spins of Fe^{3+} from LFO and the spins of Ni^{2+} from NFO may attribute in the enactment at the bulk interface. The estimated magnetic contribution of LFO and NFO grains in composite by Vegard's law are different than the observed ones. It is clear evidence of spin reconstruction at interface. The mechanism is visualized as (Fig 5) the uncompensated spin alignment at the interface, which gives rise to the enhancement, while compensated leads to decrement, which is tuned by LFO:NFO interface ratio and respective grain distribution across the interface..

Temperature profile of magnetization (M-T curve) of LFO, NFO and LFO-NFO composites are studied for fields H~500 and 1000 Oe respectively. Fig 6 shows M-T curve at magnetic field 500 Oe. The magnified view of M-T curve of LFO [see Fig 6(b)] clearly exhibits that magnetization decreases with temperature. The rapid drop of magnetization is

,

observed near anti-ferromagnetic transition temperature (T_N ~ 744K). This behavior of M-T curve shows that presence of weak ferromagnetic component, which is associated with Fe^{3+} AFM ordering.[44] The composites effect on transition temperature of LFO is predicted from derivative plot of magnetization with respect to temperature [see Fig 6(c)]. Derivative plot of magnetization of LFO [Inset Fig.6(b)] clearly displays T_N of LFO is at ~744 K. However, T_N is found to shift lower temperature side about 600 K for 80LFO-20NFO composite. For 70LFO-30NFO and 60LFO-40NFO T_N are found around 617 and 667, respectively [see Fig.6(c)]. The decrease in T_N of LFO-NFO composite can be assigned to (i) lattice parameter mismatch, which induces the mechanical strain at the interface between LFO and NFO component phases as reported elsewhere for composite system[45] and (ii) the superexchange interaction between AFM coupled Fe^{3+} ions (Fe^{3+}— O^{2-}—Fe^{3+}) in LFO get weakened due to NFO phase. However, with increasing NFO concentration in composite, T_N shift towards higher side may be due to higher magnetic transition temperature of NFO, which is around ~850 K. Hence, with increment in NFO concentration, transition temperature increases but not higher than T_N of LFO because still LFO phase is dominating in the composite samples [Fig.6(c)].

In addition to that, broadening of peak corresponds to Neel temperature (T_N) is observed with the inclusion of NFO into LFO. Broadening at T_N has been earlier observed in case of composite and doping effect and found very sensitive to composition as well as chemical ordering.[46-49] The broadening observed in current work can be assigned to in-homogenity arises in LFO matrix by NFO. With respect to NFO composition, inhomogenity increases and much broader peak is detected for 60LFO-40LFO composition. M-T curve [Fig. 6(d)] for NFO is nearly same as LFO. Magnetization is found reducing with increase of temperature and reached towards lower value at curie temperature (T_c). This is the feature of ferromagnetic or ferrimagnetic materials. Derivative plot of magnetization for NFO [inset of Fig. 6(d)] gives curie temperature ~882 K i.e. transition temperature from ferrimagnet to paramagnet. Same behavior is observed in temperature dependence magnetization of LFO, NFO and LFO-NFO composites at H=1000 Oe also. [See Fig.S1 of supplementary file].[29]

C. Mossbauer Spectroscopy

To probe local magnetic behavior of composites, room temperature Mossbauer spectra are studied. Raw Mossbauer experimental data are fitted with NORMOS-SITE DOS based program. Fig. 7 shows ^{57}Fe Mossbauer spectrum of LFO. Raw data is fitted with one sextet (which is the feature of AFM ordering in LFO) along with singlet.[50] Various hyperfine

,

parameters are obtained with respect to natural iron from fitted spectra. Isomer shift (δ) provides direct information about electron density at nucleus. δ is found to be ~0.2405 which indicates Fe in +3 state.[51] Quadrupole splitting (Δ) reflects interaction between nuclear quadrupole and surrounding electric field. Hyperfine magnetic field (B_{hf}) is the effective magnetic field which gives information about interaction between nucleus and surrounding magnetic field. Obtained hyperfine parameters corresponding to sextet and singlet for LFO, are as shown in Table 2. All these values are the characteristics of octahedrally coordinated high spin Fe^{3+}.[32,52,53] Along with highly intense sextet, a weak singlet is also detected. The relative area of that singlet is less than 1%. In literature, such Isomer shift (0.049 mm/s) observed for singlet has been correlated to superparamagnetic state of Fe by Saverio Braccini et al 2013.[54] In our work, isomer shift of this single line is found exactly correspond to superparamagnetic state of Fe. Therefore the singlet can be assigned to superparamagnetic state of Fe. As the line is very less intense, it means that very few Fe (less than 1%) are at superparamagnetic state. The state of Fe is not very prominent in our case. It is well known that LFO is superparamagnetic at room temperature (T.Fujii et al 2011).[55] Fig. 7(b) shows Mossbauer spectrum of spinel NFO. This spectra should have to be fitted with ferrimagnetic two sextets (one for tetrahedral Fe and other for octahedral), but due to broadening, only one ferrimagnetic sextet is fitted with our raw data. Various hyperfine parameters corresponds to NFO are tabulated in Table 2 and found close to the values reported elsewhere.[56-58] Mossbauer spectrum of 60%LFO-40%NFO fitted with two sextets, one is corresponding to LFO and other is for NFO. Relative areas for LFO and NFO phases (from Table 2) are found to be 59.61 and 40.39%, respectively. This confirms the exact phase proportion in our prepared composite. Hyperfine parameters for both the sextets are shown in Table 2.

Conclusions

In summary, we have developed composites of perovskite oxide ($LaFeO_3$) and spinel ($NiFe_2O_4$) to study interface effect on bulk magnetic behavior in view of enhancement of magnetization of LFO. Formation of composite is confirmed by X-ray diffraction and FTIR studies. Pervoskite-spinel interface effect on magnetic behaviour of LFO-NFO bulk composites is confirmed by M-H and M-T behaviours. Noticeable enhancement in magnetization of LFO dominant composite system is observed. The spin-coupling mechanism at the interface of pervoskite-spinel composite is proposed to understand the effect. Shifting in magnetic transition temperature with increase of NFO composition in LFO

,

is explained on basis of lattice parameter mismatch and weakening of superexchange interaction in LFO by NFO. Local magnetic behavior and phase proportion are confirmed by Mossbauer spectroscopic technique. The work demonstrates that the Pervoskite-spinel interface approach have potential to enhance the magnetization of LFO.

Acknowledgements

We acknowledge UGC-DAE Consortium for Scientific Research, Indore (India), for providing Magnetic, Mossbauer and FTIR characterization facilities and also financial support through travel assistance and local hospitality. We are grateful to Dr. R.J.Choudhary and Mr. Pankaj Pandey for their help in magnetic measurements. We would like to thank Mr. U. P. Deshpande, Scientist, UGC-DAE CSR, Indore for his help in recording FTIR spectra. We express our sincere thank to Dr. V.R.Reddy and Mr.Anil for their help in recording Mossbauer spectra and its analysis. One of the author VMG wants to acknowledge UGC, New Delhi for providing financial assistance through RGNF fellowship.

References

1 J.P.Zhou, L.Lv, Q.Liu, Y.X.Zhang, and P.Liu, Sci.Technol.Adv.Mater., 2012, **13**, 045001.

2 Q.Zhan, R.Yu, S.P.Crane, H.Zheng, C.Kisielowski, and R.Ramesh, Appl. Phys. Lett., 2006, **89**, 172902.

3 A.P.Sutton, and R.W.Ballufi, Interfaces in Crystalline Materials (Clarendon) Oxford, 1995, pp.240.

4 R.Ramesh, Current science, 2013, **105**, 1107-1114.

5 S.Pillai, D.Bhuwal, A.Banerjee, and V.Shelke, Appl.Phys.Lett., 2013, **102**, 072907.

6 J.Hoffmann et al, J.Mater.Res., 2012, **27**, No.11.

7 R. Muralidharan, N. Dix, V. Skumryev, M. Varela, F. Sánchez, and J. Fontcuberta, J.Appl.Phys**.**, 2008**, 103**, 07E301.

8 Xian-Ming Liu, Shao-Yun Fu, Chuan-Jun Huang, Materials Science and Engineering B, 2005, **121,** 255–260.

9 C.H. Yang, F. Yildiz, S.H. Lee, Y. H. Jeong, U.Chon, and T.Y.Koo, Appl. Phys. Lett., 2007, **90**, 163116.

10 R. Y. Zheng, J. Wang, and S. Ramakrishna, J. Appl. Phys., 2008, **104** , 034106.

11 S.P. Crane, C. Bihler, M.S. Brandt, S.T.B. Goennenwein, M. Gajek, and R. Ramesh, Journal of Magnetism and Magnetic Materials, 2009, **321**, L5 –L9.

,

12 K.Sone, S.Sekiguchi, H.Naganuma, T.Miyazaki, T.Nakajima, and S.Okamura, J. Appl. Phys., 2012, **111**, 124101.

13 C.M. Kanamadi, J.S. Kim, H.K. Yang, B.K. Moon, B.C. Choi, and J.H. Jeong, Appl.Phys. A, 2009, **97**, 575–580.

14 Y.Zhang, C.Deng, J.Ma, Y.Lin, and C-W. Nan, Appl. Phys. Lett., 2008, **92** , 062911.

15 R.Liu, Y.Zhao, R.Huang, Y.Zhao, and H.Zhou, J. Mater. Chem., 2010, **20**, 10665–10670.

16 K.Ueda, H.Tabata, and T.Kawai, Phys.Rev.B, 1999, **60**, R12561.

17 Y.B. Chen, J.Zhou, S-T. Zhang, F-X. Wu, S-H. Yao, Z-B.Gu, D.Wu, and Y-F.Chen, Appl. Phys. Lett., 2013, **102**, 042403.

18 R.Koferstein, and S.G.Ebbinghaus, Solid State Ionics, 2013, **231**, 43-48.

19 D.Wang, and M.Gong, J.Appl.Phys., 2011, **109**, 114304.

20 M.Idrees, M.Nadeem, M.Mehmood, M.Atif, K.H.Chae, and M.M.Hassan, J.Phys.D: Appl.Phys., 2011, **44**, 105401.

21 D.Wang, X.Chu, and M.Gong, Nanotechnology, 2006, **17**, 5501-5505.

22U.Luders, A.Barthelemy, M.Bibes et al, Adv.Mater., 2006, **18**, 1733-1736.

23S.E.Shirsath, S.S.Jadhav, B.G.Toksha, S.M.Patange, and K.M.Jadhav, J.Appl.Phys., 2011, **110**, 013914.

24 M.Younas, M.Nadeem, M.Atif, and R.Grossinger, J.Appl.Phys., 2011, **109**, 093704.

25 S.M.Patange, S.E.Shirsath, G.S.Jangam, K.S.Lohar, S.S.Jadhav, and K.M.Jadhav, J.Appl.Phys., 2011, **109**, 053909.

26 K.V.P.M.Shafi, Y.Koltypin, A.Gedanken, R.Prozorov, J.Balogh, J.Lendvai, J.Felner, J.Phys.Chem.B, 1997, **101**, 6409-6414.

27 Y.Shi, J.Ding, Z.X.Shen, W.X.Sun, and L.Wang, Solid State Communication, 2000, **115**, 237-241.

28 I.S. Smirnova, A .V. Bazhenov, T.N. Fursova, A .F. Dubovitskii, L.S. Uspenskaya, M.Yu. Maksimuk, Physica B, 2008, **403**, 3896-3902.

29 Supplimentary content, Fig.S1 Comparative temperature dependence magnetization at field 1000O e for LFO-NFO composites.

30 M.Romero, R.W.Gomez, V.Morquina, J.L.Perez-Mazariego, and R.Escamilla, Physica B, 2014, **443**, 90-94.

31 R. A. Lewis, A. D. Martin, X. L. Wang and S. X. Dou, Aust. J. Phys., 1999, **52**, 197-203.

32 M. Sivakumar, A.Gedanken, W.Zhong, Y.H.Jiang, Y.W.Du, I.Brukental, D. Bhattacharya, Y. Yeshurun, and I. Nowik, J. Mater. Chem., 2004, **14**, 764–769.

,

33 M.A. Ahmed, R. Seoudi, and S.I. El-dek, Journal of Molecular Structure, 2005, **754**, 41–44.

34 B. Senthilkumar, R. K. Selvan, P. Vinothbabu, I. Perelshtein, A. Gedanken, Materials Chemistry and Physics, 2011, Article in press.

35 Z. H. Zhou, J. M. Xue, J. Wang, H. S. O. Chan, T. Yu, and Z. X. Shen, J. A,pl. Phys., 2002, **91**, 6015.

36 N.Kasapoglu, A.Baykal, M.S.Toprak, Y.Koseoglu, and H.Bayrakdar, Turk J.Chem, 2007, **31**, 659-666.

37 S. Rana, A. Gallo, R.S. Srivastava, and R.D.K. Misra, Acta Biomaterialia, 2007, **3**, 233–242.

38 X. Li, G.Tan, W. Chen, B. Zhou, D. Xue, Y.Peng, F. Li, N. J. Mellors, J. Nanopart. Res., 2012, **14**, 751.

39 S.Singh, M.Singh, N. K. Ralhan, R. K. Kotnala, K. C. Verma, Adv. Mat. Lett., 2012, **3(6)**, 504-506.

40 H.M. Zaki, S.F. Mansour, Journal of Physics and Chemistry of Solids, 2006, **67**, 1643–1648.

41 M.A.Ahmed, S.I.El-Dek, Material Science and Engineering B, 2006, **128**, 30-33.

42 M.A.Ahemed, N. Okasha, B. Hussein, Journal of Magnetism and Magnetic Materials, 2012, **324**, 2349–2354.

43 M.B.Bellakki, V.Manivannan, P.McCurdy, and S.Kohli, Journal of Rare Earths, 2009, **27**, 691.

44 R.Rajagukguk, D.G.Shin, and B.W.Lee, Journal of Magnetics, 2011, 16, 101-103.

45 M. Murakami, K.-S. Chang, M. A. Aronova, C.-L. Lin, Ming H. Yu, J. H. Simpers, M. Wuttig, I. Takeuchi, C. Gao, B. Hu, S. E. Lofland, L. A. Knauss, and L. A. Bendersky, Appl. Phys. Lett., 2005, **87**, 112901.

46 A.Sharoni, O.Millo, G.Leitus, and S.Reich, J.Phys.:Condens.Matter, 2001, 13,L503.

47. R. Mazumder, S. Ghosh, P. Mondal, Dipten Bhattacharya, S. Dasgupta, N. Das, A. Sen, A. K. Tyagi, M.Sivakumar, T. Takami, and H. Ikuta, J. Appl. Phys., 2006, 100 , 033908.

48 P.Kushwaha, P.Bag, R Rawat and P.Chaddah, J. Phys.: Condens. Matter, 2012, 24 096005.

49. M.Halder, S.M.Yusuf, and M.D.Mukadam, Phys.Rev.B, 2010, 81, 1744022.

50 T.Fujii, I. Matsusue, M.Nakanishi, and J. Takada, Hyperfine Interact, 2011, DOI 10.1007/s10751-011-0423-4 .

51 M.Sorescu, T.Xu, J. D. Burnett, and J. A. Aitken, J Mater Sci., 2011, **46**, 6709–6717.

,

52 D.Kothari, V.R.Reddy, A. Gupta, D.M.Phase, N.Lakshmi, S.K.Deshpande, and A.M. Awasthi, J. Phys.: Condens. Matter, 2007, **19,** 136202.

53 M. Eibschut, S. Shtrikma and D. Treves, Phys. Rev., 1967, **156**, 562.

54. Braccini, O. Pellegrinelli, and K. Krämer, World Journal of Nuclear Science and Technology, 2013, 3, 91-95.

55 T. Fujii, I. Matsusue, M. Nakanishi, and J. Takada, Hyperfine Interact, 2012, 205, 97-100.

56 A.S. Albuquerque, J.D.Ardisson, W.A.A. Macedo, J.L.Lòpez, R. Paniago, A.I.C. Persiano, Journal of Magnetism and Magnetic Materials, 2001, 226-230, 1379-1381.

57 A.S. Albuquerque, J.D. Ardisson, W.A.A. Macedo, T.S. Plivelic, I.L. Torriani, J. Larrea, and E.B. Saitovitch, Journal of Magnetism and Magnetic Materials, 2004, 272–276, 2211–2213.

58 M. I. Oshtrakh, M. V. Ushakov, B. Senthilkumar, R. K. Selvan, C. Sanjeeviraja, I. Felner, and V. A. Semionkin, Hyperfine Interact, 2013, 219, 7–12.

Figure caption:

1. (a) Combined X-ray diffraction pattern of LFO, NFO and LFO-NFO composites, (b) broadening of LFO peaks with increasing NFO concentration, and (c) appearance of ferrites phase with increasing NFO percentage in composites.

2. Rietveld fitted XRD data of (a) LFO and (b) NFO

3. FTIR spectra of LFO, NFO and LFO-NFO composites.

4. (a)Field dependence magnetisation of LFO and LFO-NFO composites at RT, (b) Magnified view of MH of LFO and (c) 60%LFO-40%LFO composite

5. Mechanism of spin alignment at interface of LFO-NFO.

6. (a) Temperature dependence magnetisation of LFO and LFO-NFO composites at 500 Oe, (b) magnified view of M-T curve of LFO, inset fig shows dM/dT vrs T plot of LFO and (c)dM/dT vrs T plot of LFO-NFO composite.

7. Mossbaur spectra of (a) LFO (b) NFO and (c) LFO-NFO composite

,

Table caption:

1. Table showing various magnetic parameters of LFO, NFO and LFO-NFO
2. Hyperfine parameters from mossabaur spectra of LFO, NFO and LFO-NFO

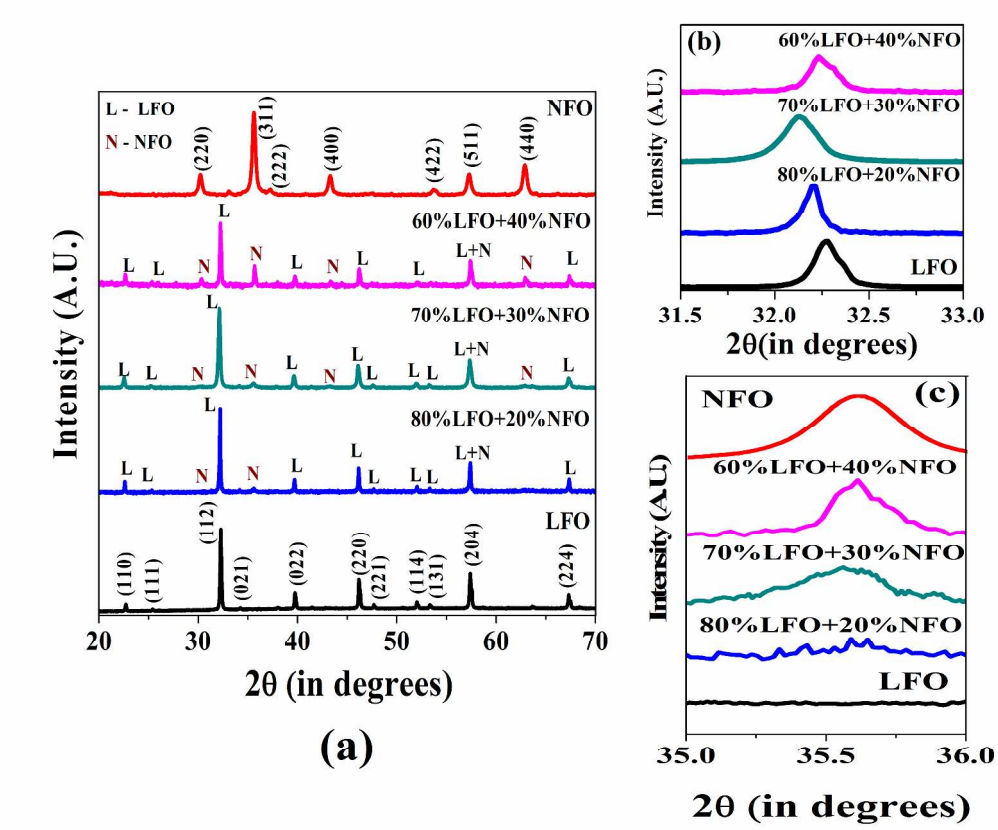

(a) Combined X-ray diffraction pattern of LFO, NFO and LFO-NFO composites, (b) broadening of LFO peaks with increasing NFO concentration, and (c) appearance of ferrites phase with increasing NFO percentage in composites.
355x304mm (300 x 300 DPI)

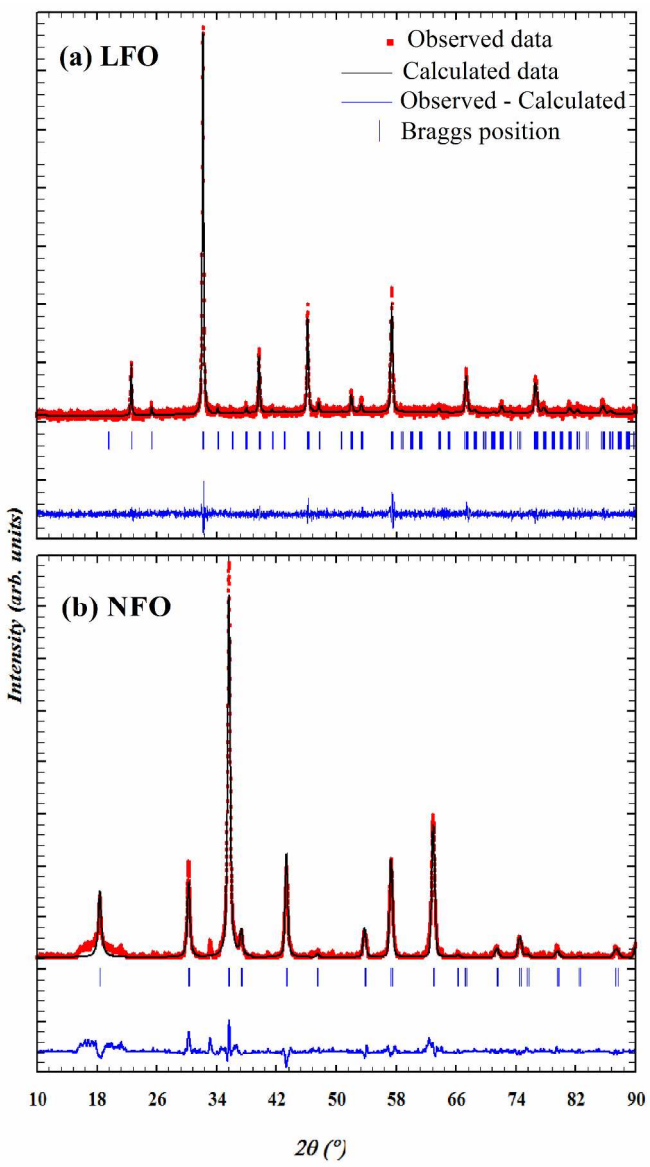

Rietveld fitted XRD data of (a) LFO and (b) NFO
254x431mm (300 x 300 DPI)

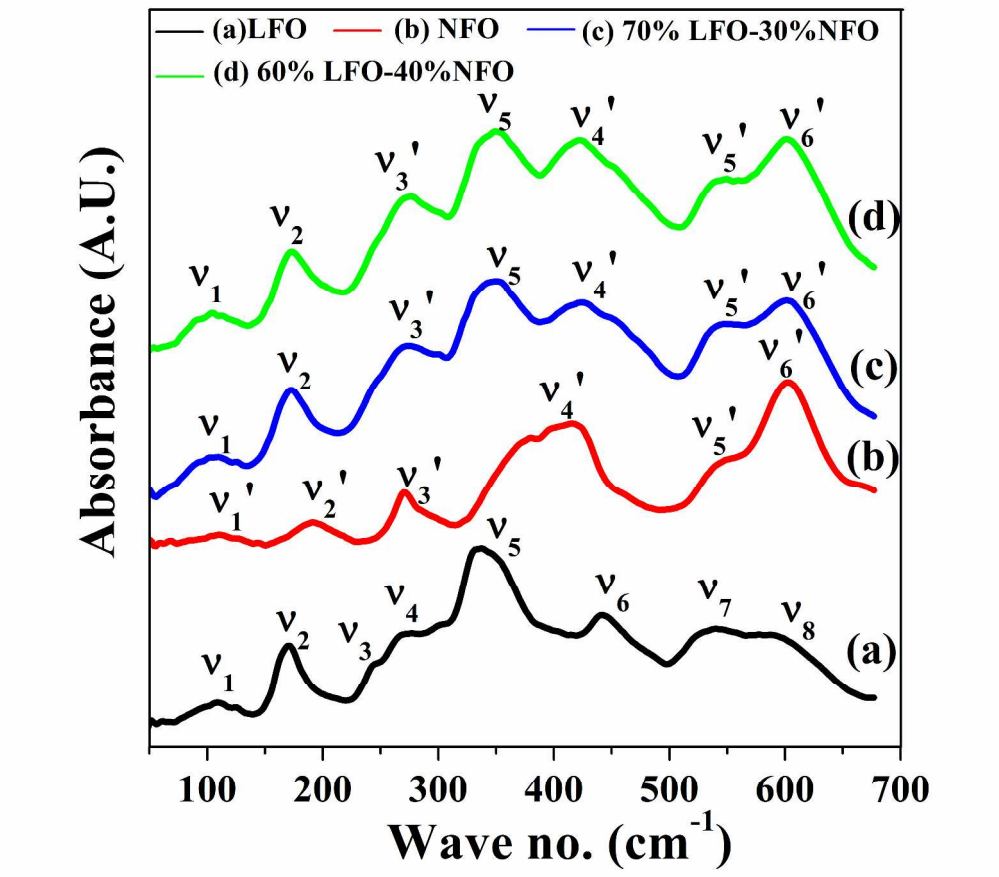

FTIR spectra of LFO, NFO and LFO-NFO composites.
355x313mm (300 x 300 DPI)

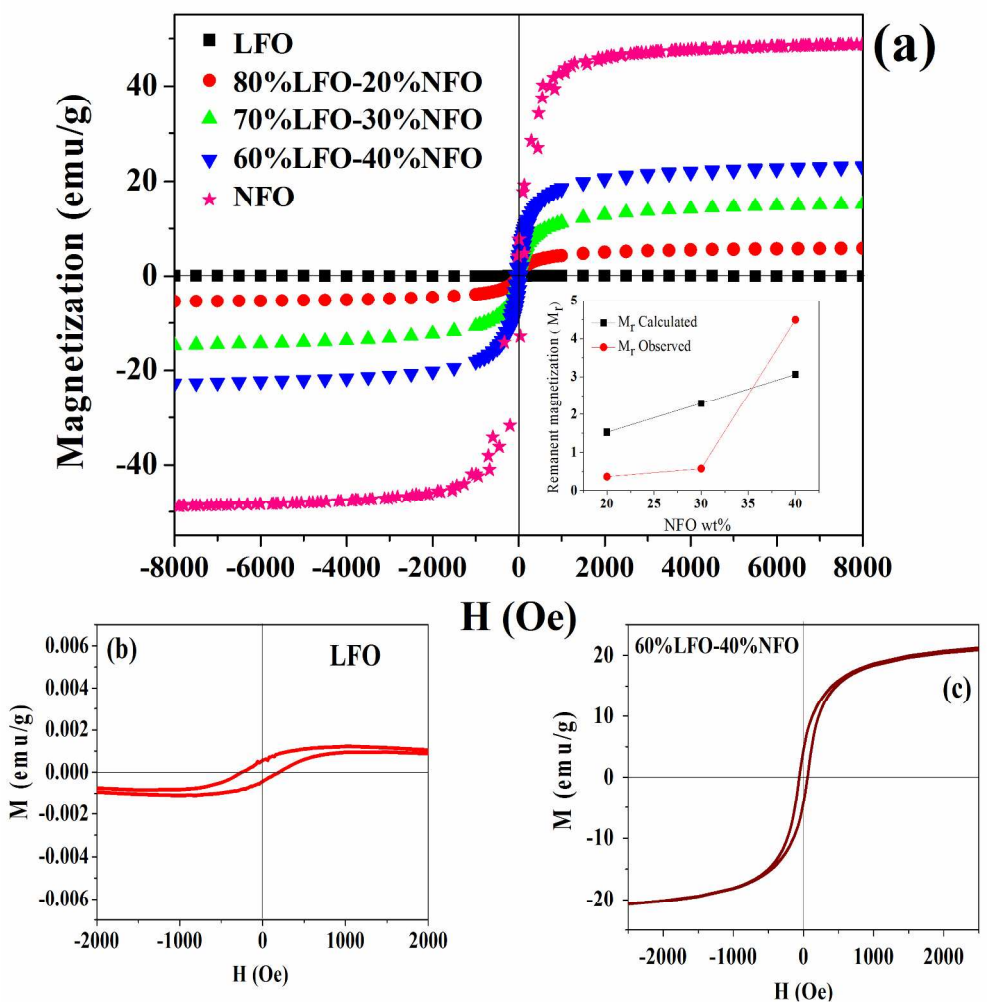

4. (a)Field dependence magnetisation of LFO and LFO-NFO composites at RT, (b) Magnified view of MH of LFO and (c) 60%LFO-40%LFO composite

254x254mm (300 x 300 DPI)

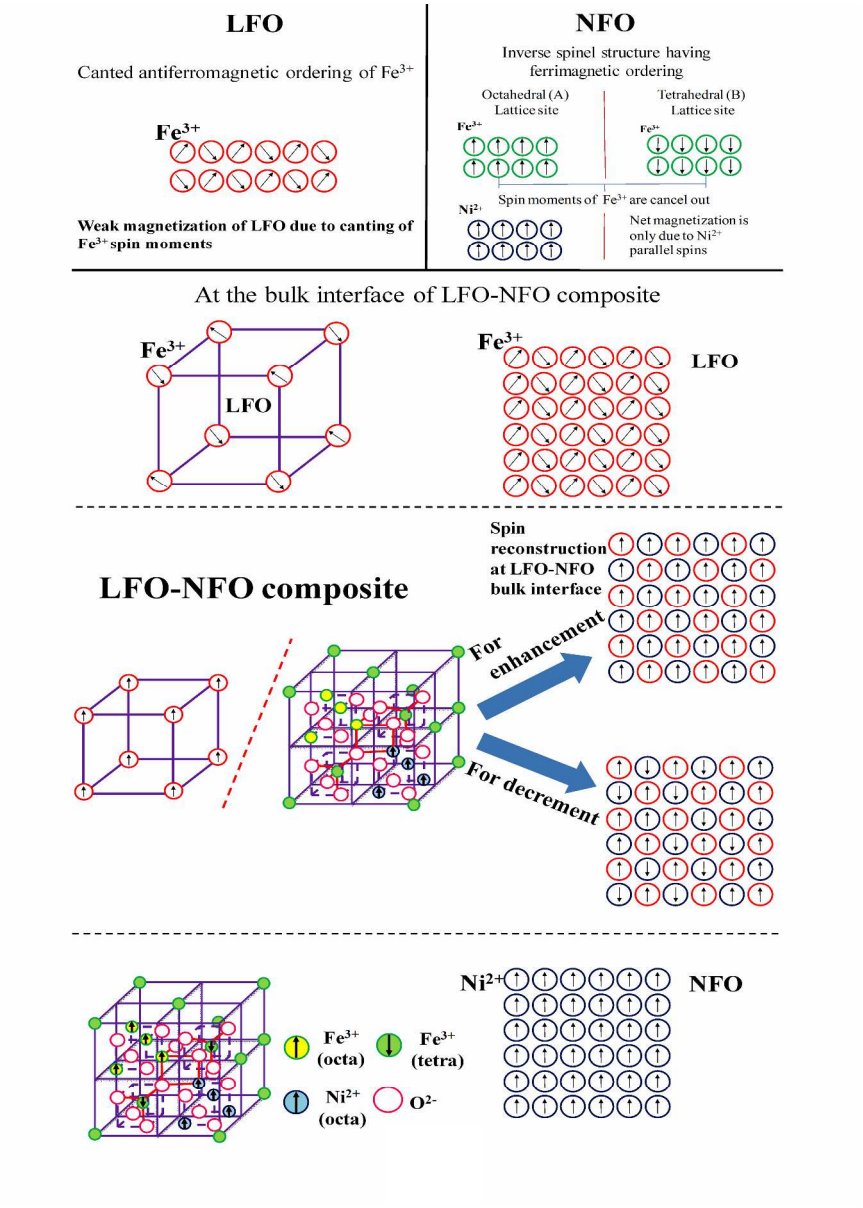

Mechanism of spin alignment at interface of LFO-NFO.
364x508mm (300 x 300 DPI)

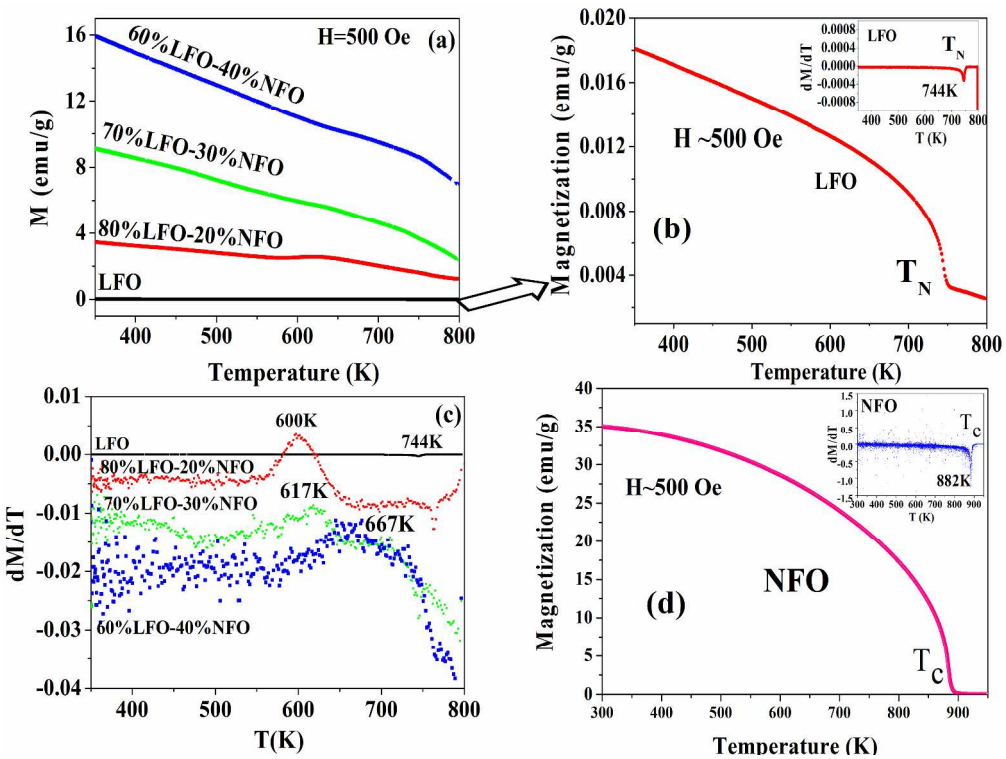

(a) Temperature dependence magnetisation of LFO and LFO-NFO composites at 500 Oe, (b) magnified view of M-T curve of LFO, inset fig shows dM/dT vrs T plot of LFO and (c)dM/dT vrs T plot of LFO-NFO composite.
381x285mm (300 x 300 DPI)

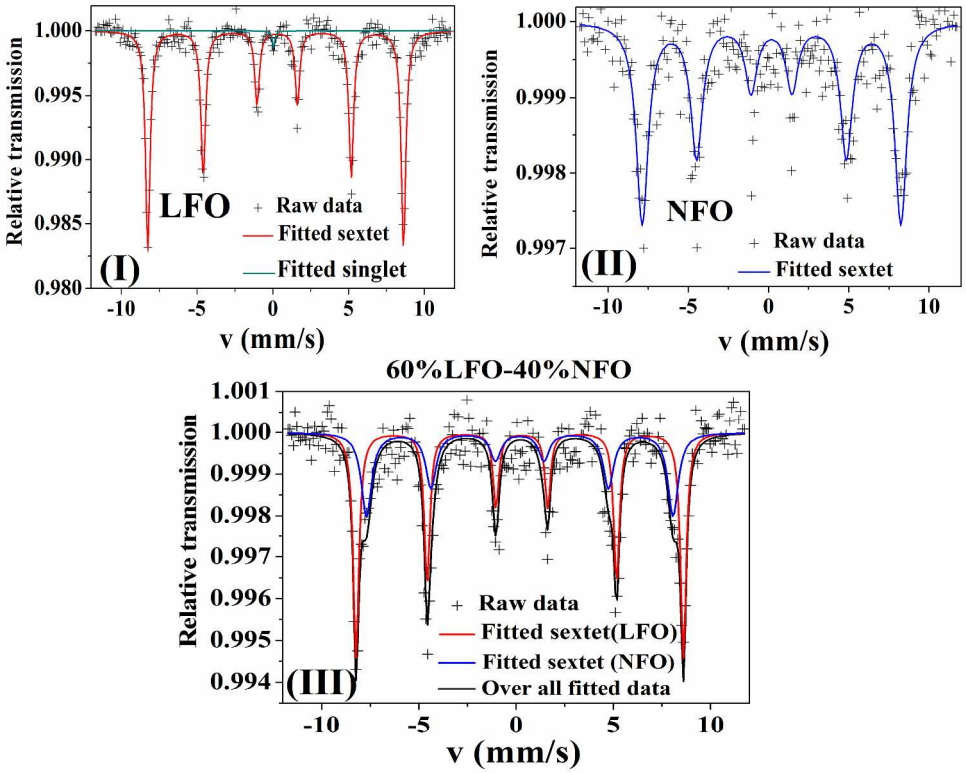

Mossbaur spectra of (a) LFO (b) NFO and (c) LFO-NFO composite
413x383mm (300 x 300 DPI)

	M_s (emu/g)	M_r (emu/g)	H_c (Oe)	$R=M_r/M_s$
LFO	0.0012	0.0005	250	0.416
80%LFO-20%NFO	5.86	0.37	20	0.063
70%LFO-30%NFO	15.58	0.57	10	0.036
60%LFO-40%NFO	23.15	4.49	60	0.193
NFO	48.80	7.65	101	0.157

Table showing various magnetic parameters of LFO, NFO and LFO-NFO
215x127mm (150 x 150 DPI)

Sample		Isomer shift (mm/s)	Quadrupole splitting (mm/s)	Hyperfine field (T)	Area (%)
$LaFeO_3$ (LFO)	Sextet	0.2405±0.0029	0.1039±0.0056	52.289±0.019	99.04
	Singlet	0.0492±0.0051	-	-	0.96
80%$LaFeO_3$-20%$NiFe_2O_4$	Sextet I(LFO)	0.2168±0.0122	0.1077±0.0273	52.373±0.101	84.87
	Sextet II(NFO)	0.0624±0.0101	0.1554±0.1027	47.428±0.312	15.13
70%$LaFeO_3$-30%$NiFe_2O_4$	Sextet I(LFO)	0.2488±0.0054	0.0732±0.0167	52.124±0.071	76.12
	Sextet II(NFO)	0.1562±0.0460	0.1742±0.0746	49.310±0.434	23.88
60%$LaFeO_3$-40%$NiFe_2O_4$	Sextet I(LFO)	0.2379±0.0073	0.1085±0.0138	52.140±0.054	59.61
	Sextet II(NFO)	0.1852±0.0261	0.0032±0.0051	48.839±0.257	40.39
$NiFe_2O_4$ (NFO)	Sextet	0.1868±0.0179	0.0032±0.0041	49.904±0.112	100

Hyperfine parameters from mossabaur spectra of LFO, NFO and LFO-NFO
215x127mm (150 x 150 DPI)